10th International Conference on Fracture Mechanics of Concrete and Concrete Structures
FraMCoS-X
G. Pijaudier-Cabot, P. Grassl and C. La Borderie (Eds)
https://doi.org/10.21012/FC10.234286

CRACKING OF REINFORCED CONCRETE STRUCTURES: A SIMPLIFIED APPROACH FOR THE GUSSET OF THE VERCORS MOCK-UP AT EARLY AGE

JACKY MAZARS[*], STEPHANE GRANGE[†] AND MATTHIEU BRIFFAUT[*]

[*] Univ. Grenoble Alpes, CNRS, Grenoble INP, 3SR, F-38000 Grenoble, France
e-mail: jacky.mazars@3sr-grenoble.fr & matthieu.briffaut@3sr-grenoble.fr

[†] Univ. Lyon, INSA-Lyon, GEOMAS, F-69621 Villeurbanne cedex, France
e-mail: stephane.grange@insa-lyon.fr

Key words: Damage and cracking models, THM modeling, Reinforced Concrete, Early age.

Abstract: VeRCoRs is a research program organized around tests performed on a mock-up of a reactor containment building at scale 1/3rd. A lot of measurements are collected since pouring of concrete and predictive calculations were made in the framework of an international benchmark. The aim of this work is to propose a simplified but efficient modelling approach for simulating the behavior of the gusset of the mock-up and particularly for predicting the cracking at early age. Simplification is based on an approach where the calculation imposes diffuse damage. The dialogue between the situation of diffuse damage and that of localized cracking, established on the basis of limit analysis concepts, allows providing convincing results on cracking indicators.

1 INTRODUCTION

In view of addressing concrete containment aging issue in nuclear power plant, EDF launch in 2013 the VeRCorRs program [1]. This program is based on a 1:3rd scale model of a reactor containment standing at EDF-Lab Les Renardières site, near Paris (figure 1).

The main objectives of the program are to study:

- the structural behavior at early age and during aging;
- the behavior during air-pressure tests and under severe accident conditions for which the thermo-mechanical loading is maintained for several days.
- the aging effects on leak tightness.

Two international benchmarks (2015 and 2018) have been organized allowing many teams to propose their know-how to deal with the modeling of these items.

The containment is a cylindrical object made by concrete layers. The raft was poured in a single phase on the foundation and the gusset located at the base of the containment was made in one layer on the raft already hardened. Above the gusset, the second layer of the cylindrical wall was poured several days later.

This study intends to address the issue to forecast the cracking which appears in the gusset at early age. This was favoured by a restrained shrinkage due to the raft which is a very massive reinforced concrete cylinder.

Figure 1: The VeRCoRs containment building under construction.

The first benchmark (2015) was mainly focused on the behaviour of the structure during the construction phase and in particular on that of the gusset at an early age. 7 participants addressed their results. Most of them mastered thermomechanical effects during this period, but the transition to crack prediction was only addressed by 3 teams and only 2 gave quantitative results with a low concordance with respect to the measurement results [2].

On this subject, more recently, a significant work has been done by [3]. The author uses a very complete 3D modelling, including stochastic variabilities useful to locate cracks, but requiring several realizations to access the average cracking mode. The cost of such an approach makes it unaffordable and leads the author to defend the interest of alternative methods.

In this context, we propose below to revisit the way to approach cracking prediction in situations where the stress field is almost homogeneous (tension in a beam or in an axisymmetric reinforced concrete shell).

2 CRACKING ANALYSIS OF A TIE

Several authors have worked on the progressive cracking of reinforced concrete tie rods, mainly to study the main cracking indicators (spacing, opening,...) [4], but also to analyze the details of crack formation (local strain evolution, progressive debonding…) [5]. These studies were mainly used to develop formulas for crack spacing and crack opening presented in the model code [6]. In the same time, finite element calculations, using smeared concrete models, were used to simulate the progressive cracking of reinforced concrete ties. These calculations are not trivial; to reproduce the cracking distribution they imply to introduce, in addition to refined models, some stochastic approaches [7]. This makes the analysis more complex and lengthy.

The idea here is to greatly simplify the approach. On the basis of damage modelling, the calculation is carried out assuming a diffuse distribution of damage. At a given stage of the load, the result gives a constant value for stress, strain and damage throughout the structure.

This scheme gives results on average. In parallel, reality is approached from the *limit analysis* concepts, based here on the use of a *cracking scheme*, which respects static equilibrium and kinematic compatibilities. In this context, some assumptions are taken into account, as shown in figure 2 for the cracking process described:

- cracks are regularly distributed, s_c being the crack spacing;
- at the level of a crack, considered transversal, the concrete stress is assumed to be nil and the stress in the rebar reaches a peak value;
- On both parts of the crack, the stress evolves, upward for concrete, downward for reinforcement; these evolutions are assumed to be linear over a given length x_r, which is a characteristic length of the problem; outside these areas, the stress is constant for both, concrete and rebar respectively.

Then, the link between the both schemes must be done:

- the diffuse one, characterized by a mean damage d_m. This mean diffused damage must include what is due to the crack formation and what is due to the rebar-concrete debonding. This implies a specific behavior law for concrete;
- the localized one, which implies localized cracking, characterized by the spacing s_c and the characteristic length x_r

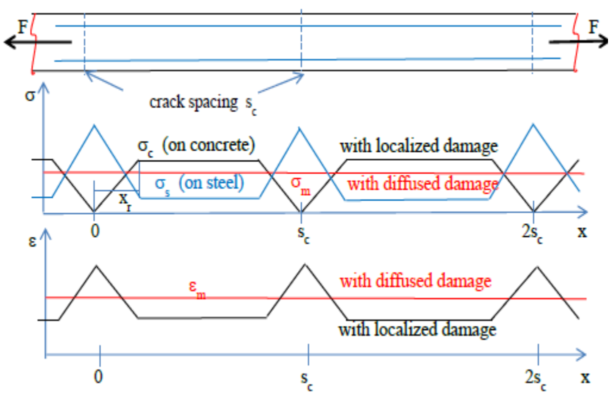

Figure 2: localized cracking and diffuse scheme (red) in a tie rod loaded in tension.

2.1 Relation between both schemes

In a limit analysis we have to ensure static equilibrium and kinematic consistency for the chosen limit state given by figure 2.

2.1.1 Static equilibrium

F is the global force supported by the whole structure, σ, A, E are the stress, the cross section and the Young modulus respectively, index s is for steel and c for concrete. ρ is the steel-concrete ratio (A_s/A_c)

Localized scheme

$\varepsilon(x)$ is the strain at location x, assumed to be the same for concrete and steel. For every x between 0 and $s_c/2$ and at a given time t, we can write:

$$F(t) = \sigma_c(x).A_c + \sigma_s(x).A_s \quad (1)$$

or, $\sigma_c(x) = F(t)/A_c - \sigma_s(x).A_s/A_c \quad (2)$

- at the level of a crack (x=0) :

$$F(t) = \varepsilon(0).E_s.A_s \quad (3)$$

- in the regularized zone ($x=s_c/2$) :

$$F(t) = \varepsilon\left(\frac{s_c}{2}\right).[E_c.A_c + E_s.A_s] \quad (4)$$

Diffused scheme

In the diffused scheme, ε_m is the strain (the same for steel and concrete) and σ_{cm} and d_m are the stress and the damage on concrete respectively:

$$F(t) = \varepsilon_m(t).[E_c.(1-d_m).A_c + E_s.A_s] \quad (5)$$

- from (2) & (5) and for $x=s_c/2$:

$$\sigma_c\left(\frac{s_c}{2}\right) = \varepsilon_m(t).E_c.(1-d_m) + \rho.E_s.\left[\varepsilon_m(t) - \varepsilon\left(\frac{s_c}{2}\right)\right] \quad (6)$$

- for x=0, σ_c is nil, then:

$$0 = \varepsilon_m(t).E_c.(1-d_m) + \rho.E_s.[\varepsilon_m(t) - \varepsilon(0)]$$

$$\rightarrow \sigma_{cm}(t) = \rho.E_s.[\varepsilon(0) - \varepsilon_m(t)] \quad (7)$$

2.1.2. Kinematic consistency

The global displacement must be the same at a given time (t) for both schemes. This can be written, for the interval [0, $s_c/2$]:

$$\varepsilon_m(t).\frac{s_c}{2} = [\varepsilon(0) + \varepsilon(x_r)].\frac{x_r}{2} + \varepsilon\left(\frac{s_c}{2}\right).\left[\frac{s_c}{2} - x_r\right] \quad (8)$$

- between x_r and $s_c/2$, ε (x) is constant, then:

$$\varepsilon_m(t) = \varepsilon\left(\frac{s_c}{2}\right).\left[1 - \frac{x_r}{s_c}\right] + \varepsilon(0).\frac{x_r}{s_c} \quad (9)$$

- (7) and (9), lead to:

$$\frac{\sigma_{cm}(t)}{\rho.E_s} = \left[1 - \frac{x_r}{s_c}\right].\left[\varepsilon(0) + \varepsilon\left(\frac{s_c}{2}\right)\right] \quad (10)$$

- but (3) and (4), lead to:

$$\varepsilon(0) = \varepsilon\left(\frac{s_c}{2}\right).\left[\frac{E_c}{\rho.E_s} + 1\right] \quad (11)$$

- mixing (9) and (11), it comes:

$$\varepsilon(0) = \varepsilon_m(t).\left[\frac{E_c}{\rho.E_s} + 1\right] / \left[1 + \frac{x_r}{s_c}.\frac{E_c}{\rho.E_s}\right] \quad (12)$$

- then (7) becomes:

$$\sigma_{cm}(t) = \varepsilon_m(t).E_c.\left[1 - \frac{x_r}{s_c}\right] / \left[1 + \frac{x_r}{s_c}.\frac{E_c}{\rho.E_s}\right]$$

- but:

$$\sigma_{cm}(t) = \varepsilon_m(t).E_c.(1-d_m) \quad (13)$$

- then:

$$(1-d_m) = \left[1 - \frac{x_r}{s_c}\right] / \left[1 + \frac{x_r}{s_c}.\frac{E_c}{\rho.E_s}\right] \quad (14)$$

Equation (14) gives the evolution of the diffused damage d_m, which is conditioned by the characteristics of the rebar-concrete composite (ρ, E_c, E_s) and is driven by the ratio x_r/s_c.

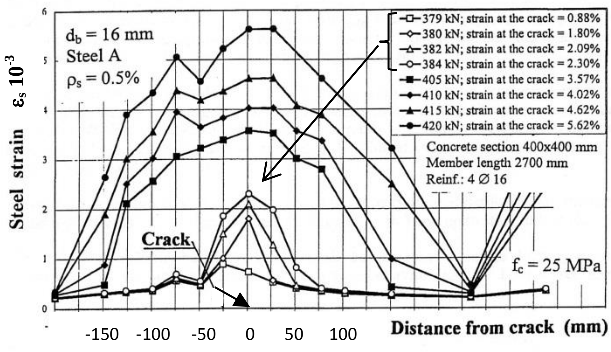

Figure 3: Rebar-concrete debonding effects, from [5]

E_c, E_s and ρ are known, x_r is the debonding length, a material characteristic which must be determine from specific experiments. From tests on ties [5], figure 3 gives the evolution of the steel strain at different stage of loading, in the vicinity of a crack. Two stages of debonding are shown: one, until 384kN, is related to the formation of the crack and one, after 405kN, is related to the opening of the crack and at the same time the yielding of rebars (ε_s>0.25%).

For the specific applications presented in this paper the first stage is the only one explored (no yielding is observed at early age). Then, assuming a fixed value for x_r during the cracking process, a given value of d_m corresponds to a unique value for the mean crack spacing s_c.

2.2 σ–ε law for the diffuse scheme

Just before the beginning of the cracking process, both stress curves (the diffuse one and the localized one) are confused and the sigma value is the tensile strength f_t.

During the cracking process this stress (f_t=$\varepsilon_{0t}.Ec$) remains constant between 2 cracks outside the debonding zones and the related strain is ε_{0t}. Then (6) becomes:

$$\varepsilon_{0t}.E_c = \varepsilon_m(t).E_c(1-d_m) + \rho.E_s[\varepsilon_m(t)-\varepsilon_{0t}] \qquad (15)$$

- which gives :

$$(1-d_m) = \frac{\varepsilon_{0t}}{\varepsilon_m(t)}.\left[1+\frac{\rho.E_s}{E_c}\right]-\frac{\rho.E_s}{E_c} \qquad (16)$$

- (16) introduced in (13) gives the following expression for the post-peak σ_{cm}–ε_m curves:

$$\sigma_{cm}(t) = E_c.\varepsilon_{0t} - \rho.E_s.[\varepsilon_m(t)-\varepsilon_{0t}] \qquad (17)$$

Then, due to the cracking scheme chosen (figure 2), one can observe on figure 4 (dashed line) that the tensile diffuse behavior is composed of two straight line, one before and one after the peak.

2.3 Application to Mivelaz ties

An experimental campaign on reinforced concrete tie sponsored by EDF, have been done at EPFL by Mivelaz [8]. We use some of these results here to validate the proposed approach. Table 1 gives the concrete characteristics for 3 ties tested with different concrete and different rebar/concrete ratio (R4, E4 & E5). For each of them, the steel Young modulus is Es=200GPa.

From (17), the post-peak tensile diffuse behavior can be set up:

- R4: σ_{cm}(t)= –1720ε_m(t)+2.64 MPa
- E4 :σ_{cm}(t)= –1720ε_m(t)+3.12 MPa
- E5 : σ_{cm}(t)= –2300ε_m(t)+3.155 MPa

Table 1: Mivelaz ties, material characteristics

Element	Rebar/concrete ratio (ρ)	Elastic modulus (GPa)	Tensile strength (MPa)
R4	0.0086	30	2.5
E4	0.0086	45	3
E5	0.0115	45	3

During the test, comparison has been performed at ε_m= 0.3%, a situation for which cracking is stabilized. At this stage and from the previous equation σ_{cm} can be calculated. Deduced from (13), the corresponding values for the diffuse damage are:
R4: d_m =0.764 - E4 d_m = 0.807 - E5: d_m = 0.817.

Finally equation (14) allows to give the related value for x_r/s_c. Assuming that x_r is in the same range as the value given by the test shown figure 3 (x_r #0.05m), we can deduced for s_c the results given table 2, which are in good accordance with experimental results.

Table 2: Crack spacing for the Mivelaz ties

Element	Experiment (m)	Calculation (m)
R4	0.27	0.33
E4	0.25	0.27
E5	0.24	0.21

Figure 4 gives, as an example, the corresponding behavior for the tie E5. The dashed line corresponds to the previously defined σ_{cm}-ε_{cm} equation and the solid line curve is a modified one to take into account the tension stiffening which appears at large deformation.

From this last curve, the overall force-displacement behavior of the tie (concrete force + rebar force) is deduced, which is compared, figure 5, with the experimental curve. This figure shows the consistency of the current simplified modelling.

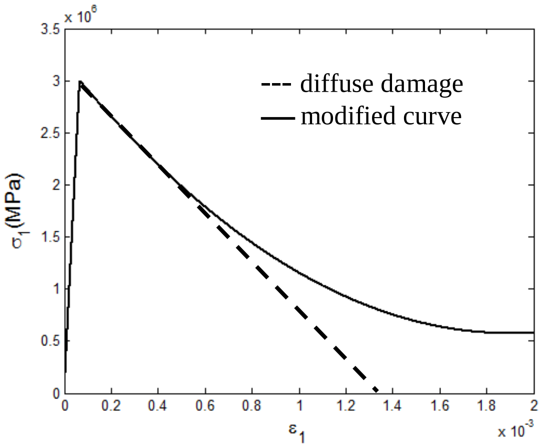

Figure 4: Dashed line, diffuse tensile behavior for the Mivelaz ties E5. Full line, modified curve to take into account the tension stiffening at large deformation.

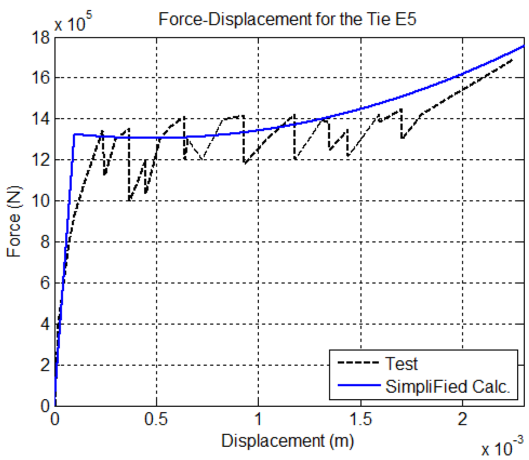

Figure 5: Force-Displacement of the Mivelaz tie E5, comparison experiment – simplified calculation.

Confident about this approach, we propose in the following to use it to forecast the cracking of the gusset VeRCoRs mock-up, bearing in mind that the cracking is directly related to the effects at early age.

3 THE VERCORS MOCK-UP

Figures 1 gives a global view of the whole VeRCoRs facilities and figure 6 a cross section of the mock-up. During the construction measurements were achieved just after concreting during time intervals of one hour. During the research program, several measurements are collected every day on each sensor. Hundreds of samples of concrete have been prepared and tested to determine material properties and behavioral parameters, including modulii and strengths, drying, shrinkage, creep, permeability…etc.

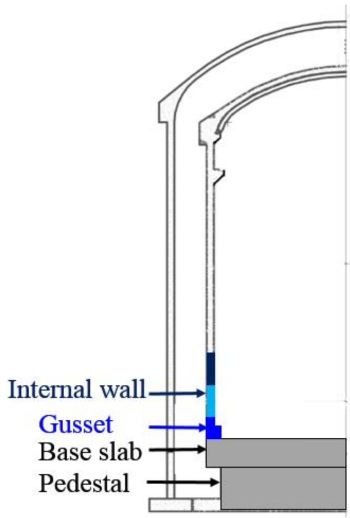

Figure 6: Location of the gusset in the whole structure.

The base slab (raft) was poured in a single phase on the pedestal and the gusset, located at the base of the containment, was made in one layer on the raft already hardened. Above the gusset, the second layer of the cylindrical wall was poured twenty days later. A few days after pouring cracks appear in the gusset. These cracks will then be closed by prestressing. The intention here is to predict, through the method described above, the occurrence of this cracking and to give its characteristics.

In comparison with the problem discussed section 2, the problem here is different for two main reasons:

1- The gusset is a circular element, that can be considered axisymmetric.

2- The loading is exclusively due to the combined effects of early age and boundary conditions; it is particularly due to strains hindered by the presence of the base slab.

From the first point, the choice was made to treat the problem in an axisymmetric way (2D). Discretization is done in a section of the gusset and the results are considered identical all around it, thus implying diffuse damage throughout the element.

The second point requires treating the THM problem from the date of pouring of the gusset to the formation of cracks (the experiment showed that they are almost stabilized after 12 days). To do this, we have resumed the work already done to simulate the behaviour of the RG8 experiment, which was a large beam whose shrinkage has been restrained by metallic struts (see [9]). As it was a beam, the problem has been treated using a multifiber beams type discretization (1D modeling). In the present case the modeling is 2D in the section of the gusset and assumed axisymmetric.

4 MODELS

At early age following phenomena are strongly coupled for reinforced concrete:

- Cement hydration;
- Thermal deformation of concrete and steel;
- Evolution of performance with maturation;
- Autogenous shrinkage of concrete;
- Basic creep of concrete;
- Elasto-damaging behavior of concrete;

The following describes how these different issues are addressed.

4.1 Thermal model for early age

Hydration is a thermo-activated phenomenon. Thus, the gusset heats up under the effect of internal heat sources, especially since it is massive (diameter 15m, height 1m, thickness 0.6m). Exhaustion of the reaction and external exchanges lead to cooling, until gradually reaching balance. At the same time the material is subjected to various volumic variations and the mechanical performance increases.

As usual, the thermal problem is treated independently of the mechanical problem and the three main equations which follows must to be solved [10].

* The energy balance equation:

$$C\dot{T} = \nabla(k\nabla T) + L\dot{\xi} \qquad (18)$$

$\dot{x} = dx/dt$, T is the temperature (K), k is the thermal conductivity (W.M^{-1}.K^{-1}), L *is* the latent hydration heat (J.m^{-3}) and C is the volumic thermal capacity (J.m^{3}K^{-1}).

* The Arrhenius equation, from which is deduced the hydration degree ξ:

$$\dot{\xi} = A(\xi)\exp(-\frac{E_a}{RT}) \qquad (19)$$

$A(\xi)$ is the chemical affinity (s^{-1}), an expression of ξ derived from Sciumé et al. [11] and in which the maturity concept presented below is introduced [12]; E_a is the activation energy (J.mol^{-1}), R is the ideal gas constant equal to 8.3145 J.K^{-1}.mol^{-1}.

* The external exchange, given by the heat flux φ (W.m^{-2}):

$$\varphi = h(T_s - T_{ext})n \qquad (20)$$

n is the vector normal to the surface, T_s is the surface temperature (K) and T_{ext} the external temperature (K). h is the exchange coefficient (W.m^{-2}.K^{-1}).

4.2 Mechanical modeling

The basis is the μ damage model [13]. Damage description is assumed to be isotropic and directly affects the stiffness evolution of the material. Let $\boldsymbol{E}$ be the stiffness matrix of the original material, then the constitutive tensorial equation is:

$$\underline{\underline{\sigma}} = \underline{\underline{\underline{\underline{\boldsymbol{E}}}}}(1-d):\underline{\underline{\epsilon}} \qquad (21)$$

d is the effective damage, a scalar driven by the variable:

$$Y = \mathrm{r}Y_t + (1-\mathrm{r})Y_c \qquad (22)$$

$Y_t = \mathrm{Max}(\varepsilon_{0t}, \max\varepsilon_t)$ and $Y_c = \mathrm{Max}(\varepsilon_{0c}, \max -\varepsilon_c)$. ε_t , ε_c are the equivalent strains cracking and crushing respectively. ε_{0t} is the tensile strain threshold and ε_{oc} is the compressive strain threshold. r is the triaxial factor [14], the expression of which is given by :

$$\mathrm{r} = \frac{\sum_i \langle\tilde{\sigma}_i\rangle_+}{\sum_i |\tilde{\sigma}_i|} \qquad (23)$$

$\tilde{\sigma} = \sigma/(1-d)$, is the effective stress. Generally ε_{0t} corresponds to the tensile strain at peak, then it can be written: $\varepsilon_{0t} = f_t/E$ (f_t being the tensile strength).

This model is suitable to describe unilateral damage (d is nil when cracks are closed and positive if they are opened). For more details see [13].

4.3 Thermo-Chemo-Mechanical coupling

The mechanical performances progressively increase with the hydration process. To describe the state of the medium, the maturity M is introduced [12]. for $\xi > \xi_0$:

$$M = \left\langle \frac{\xi - \xi_0}{\xi_\infty - \xi_0} \right\rangle_+ \qquad (24)$$

ξ_0 is the percolation threshold (close to 0) and ξ_∞ the hydration degree when the hydration reaction is over (# 0.8, from previous experiments).

M evolves from 0 (beginning of the process) to 1 (end of hydration) and is used in a simple way to forecast:

- the Young modulus : $E=M.E_\infty$, E_∞ being the value when M =1 (matured concrete);
- the tensile strength of concrete : $f_t(M) = E(M).\varepsilon_{0t}$ (ε_{0t} is constant whatever is the maturity).

These relations are a specific case of the ones proposed by de Shutter [15].

From this, it is easy to describe the non-linear behavior of the material by substituting $\boldsymbol{E}$ by $\boldsymbol{E}.M$ in the equation (21). In other words, this gives for the Young modulus at a given maturity M and a given damage d:

$$E_d(M) = E_\infty . M.(1-d) \qquad (25)$$

Global description of the problem

This description is based on the following strain superposition [9]:

$$\underline{\underline{\varepsilon}} = \underline{\underline{\varepsilon_e}} + \underline{\underline{\varepsilon_{bc}}} + \underline{\underline{\varepsilon_{au}}} + \underline{\underline{\varepsilon_{th}}} \qquad (26)$$

From which, the global behaviour is written:

$$\dot{\underline{\underline{\tilde{\sigma}}}} = \underline{\underline{\underline{\underline{\boldsymbol{E}}}}}(M):(\underline{\underline{\dot{\varepsilon}}} - \underline{\underline{\dot{\varepsilon}_{bc}}} - \underline{\underline{\dot{\varepsilon}_{au}}} - \underline{\underline{\dot{\varepsilon}_{th}}}) \qquad (27)$$

These equations are obviously tensorial, all the phenomena that are considered here are taken into account in an isotropic way. To simplify the writing we will not repeat in the following the tensorial symbolism.

$\tilde{\sigma}$ is the effective stress, then (27) introduces damage in the whole process.

ε_{th} is the thermal strain: $\quad \varepsilon_{th} = \alpha T \qquad (28)$

α being the thermal dilation coefficient (K^{-1}).

ε_{au} is the autogeneous shrinkage:

$$\varepsilon_{au} = -\kappa_\infty M \qquad (29)$$

κ_∞ being the final shrinkage (μm/m).

Creep is described by a series of three Kelving-Voigt models and the behavior of each model is given by :

$$\tau^i_{bc}\ddot{\varepsilon}^i_{bc} + (\tau^i_{bc}\frac{\dot{k}^i_{bc}(M)}{k^i_{bc}(M)} + 1)\dot{\varepsilon}^i_{bc} = \frac{\dot{\tilde{\sigma}}}{k^i_{bc}(M)} \qquad (30)$$

ε_{bc} is the basic creep.

The stiffness of each spring is on the form $k_{bc}(M) = \mathcal{A}(M)\ k_{bc\infty}$, and $\tau_{bc} = \eta/k$ is the characteristic time of a given Kelvin -Voigt model. A non-linear internal procedure is carried out inside the constitutive law to fulfill the stress equilibrium in each spring.

5 APPLICATION TO THE GUSSET

5.1 Meshing

As indicated below the gusset, is considered axisymmetric. Then the mesh is totally described by a vertical cross section of the structure and axisymmeric assumptions.

The concrete of the base slab is hardened when the gusset is poured, it is a very massive object (a cylinder with a diameter of 15m and a thickness of 2m). To simplify the problem the central part of the base slab is not meshed (figure 7). The pedestal is assumed perfectly stiff. Then, in the r, θ, z repair, a zero displacement in the z direction is imposed for the bottom part of the base slab in connection with the pedestal.

The horizontal rebars are located at their right positions in the mesh and the vertical ones are homogeneized and appears as a cylinder in the mesh (black lines in figure 6).

Then the total number of elements is :

- 66 quad4 elements for the gousset;
- 182 quad4 elements for the base slab;
- 46 elements for the vertical rebar.

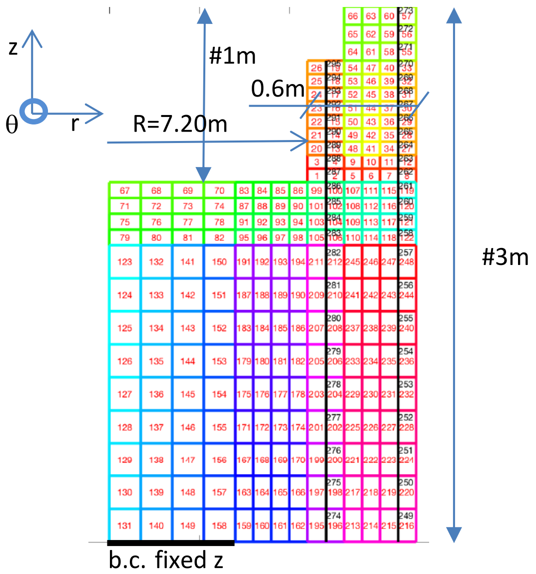

Figure 7: Mesh and boundary conditions.

5.2 Thermo-Chemo-Mechanical loading

The gusset is the first layer poured on the matured base slab and the second layer is poured twenty days after (see figure 6). The present calculation is performed during this first period [0, 12 days].

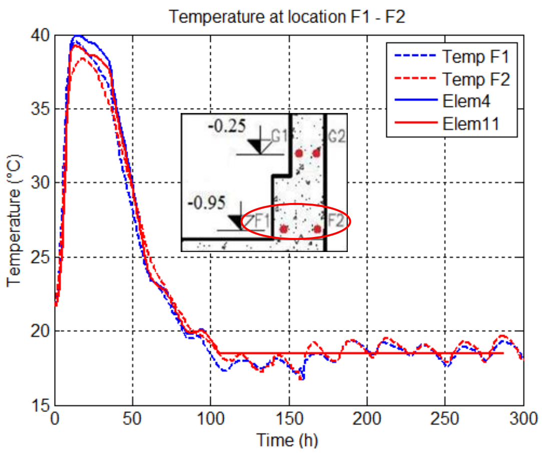

Figure 8: Temperature evolution of the Gusset during the first 12 days– comparison measures/calculations.

To recreate the thermal conditions observed during the pouring of a gusset for a real containment, a specific external temperature has been imposed:

- from 0 to 3h: Text=20°C;
- from 3h to 17h : Text=38°C;
- from 17h to 35h : Text = 48°C;
- after 35h: Text is the one measured outside the construction.

This temperature varied between night and day, to simplify it was assumed a constant mean value 18.5°C.

Figure 8 shows the results obtained, after identifying the parameters (from tests on samples), for the evolution of temperature at measured points (F1-F2) of the gusset. A very good comparison is obtained with measurements performed in situ.

5.3 Shrinkage and creep

Due to the massiveness of the structure and the relative brevity of the experiment (12 days) drying is not considered in the structure.

In this context:

- autogenous shrinkage was calibrated on previous tests performed on samples (κ_∞=150 µm/m);
- basic creep model was also calibrated on previous laboratory tests and, in order to cover in an optimized way the whole duration of the test, the characteristic times of the three Kelvin –Voigt models were: τ_1=0.1day, τ_2=1day, τ_3=10days.

5.4 Mechanical properties

From equations (19) and (24) and the temperature evolution, *M(t)* can be calculated, it is used to match the Young modulus at a given time.

Table 3: Gusset characteristics

Rebar/conc. ratio (ρ)	Steel elastic modulus (GPa)	Concrete elastic modulus at 28d. (GPa)	Tensile strength at 28days (MPa)
0.007	200	33	2.8*

*estimated from splitting tests on samples (ϕ=11cm)

As presented section 2 for the tie analysis, damage calculated in the gusset is a diffuse one, which implies an adapted damage evolution law given by equation (17). Then, using the material characteristics given table 3, the post-peak tensile diffuse behavior can be set up:

$$\sigma_{cm}(t) = -1470\varepsilon_m(t)+2.925 \text{ MPa} \qquad (31)$$

As presented section 2, the post-peak curve has been modified to take into account tension stiffening at large deformation, in the present case it was transformed into a quadratic curve that respects the post peak line determined above on the first phase of the cracking process due to the THM loading (figure 9a).

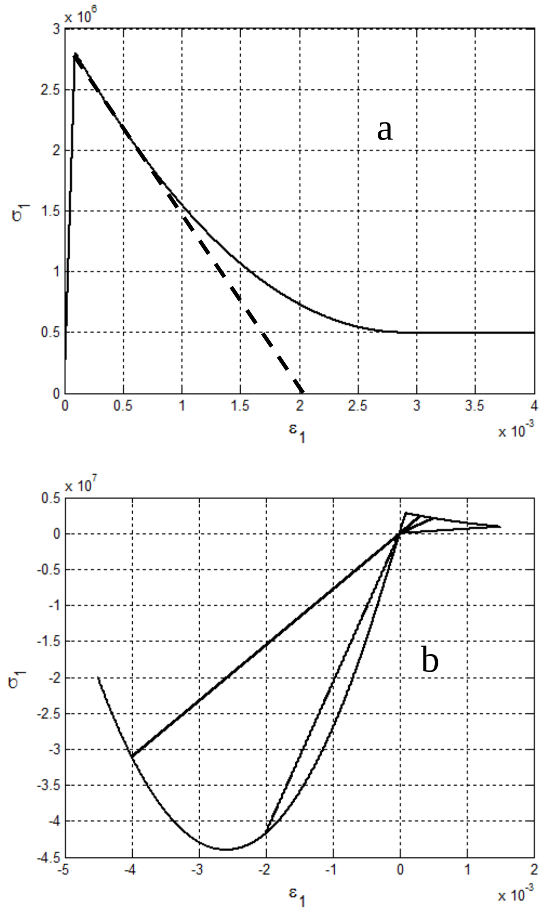

Figure 9: Response of the μ model identified for the matured concrete of the gusset; a/ tensile response; b/ cyclic uniaxial response.

Respecting the principle exposed section 4.2, equation (22) and (23), the final expression for d_m is a quadratic form of Y_m (= rY_{tm}+(1-r)Y_{cm}), Y_{tm} and Y_{cm} being the maximum value reached by ε_{tm}, ε_{cm} respectively. Figure 9b gives the uniaxial cyclic response of the model.

5.5 Results

Strain results

Strain evolved due to the combination of thermal and shrinkage effects. Measurement have been done at the same points in two direction (tangential (θθ) and vertical (zz)).

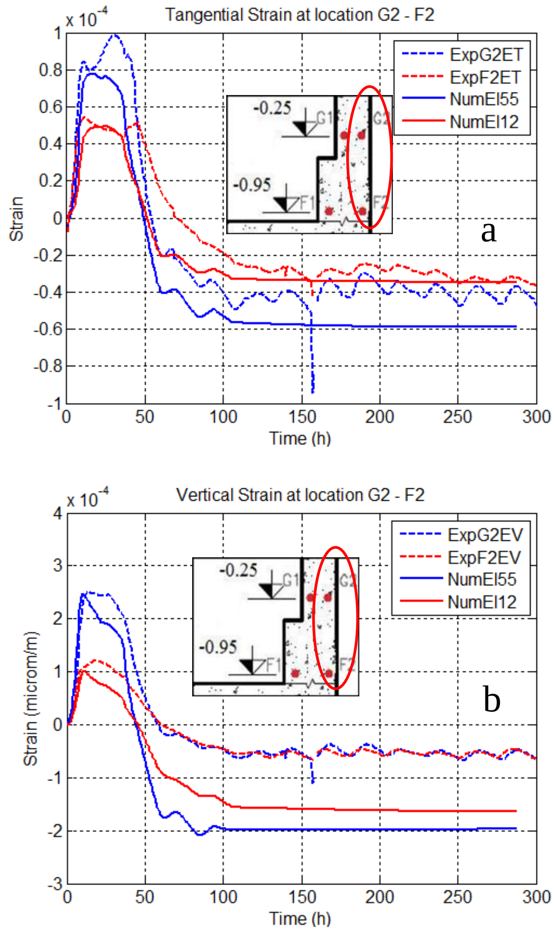

Figure 10: Strain evolution in the gusset during the first 12 days– comparison measures (dashed lines) /calculations (full line): a/ Tangential strain; b/ Vertical strain.

Figure 10 gives the comparison calculation/measures for tangential strains (figure 10a) and vertical strain (figure 10b). The results are globally good apart after 50 hours for which the vertical ones are overestimated.

Damage results

As presented in section 4.2, the calculation gives the axisymmetric diffused damage d_m. Figure 11 gives the damage field showing that the gusset is the only part damaged. The bottom part of the gusset is a sensitive part due to the effect of the base slab which restrained the shrinkage of the gusset. This generate on both side two locations of relatively high damage, prefiguring the onset of possible horizontal cracks. Vertical cracks (observed during experiment) are related to the diffuse damage value in the core of the gusset which is, at 12 days in mean value, d_m # 0.55 (figure 11b).

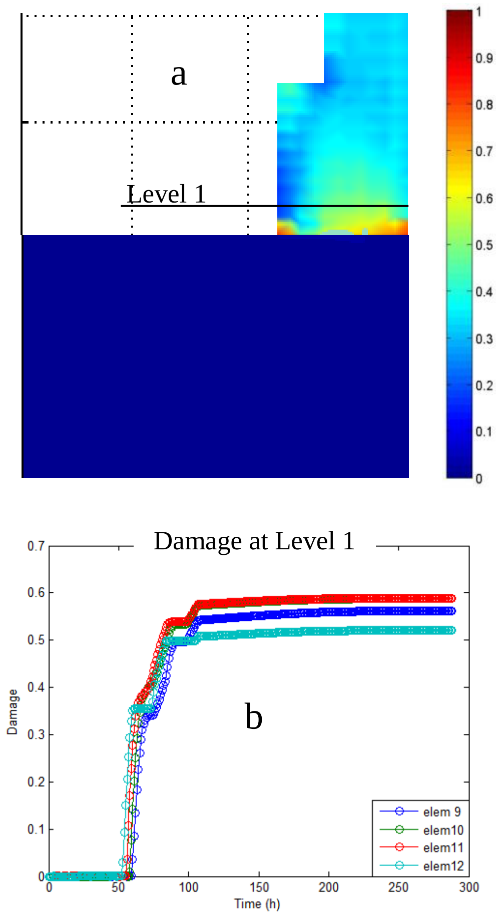

Figure 11: Damage in the Gusset due to maturation effects; a/ Damage field; b/ Damage evolution inside the gusset at level 1.

Equation (14) gives the link between d_m and the ratio x_r/s_c. Without any specific results for x_r, we have taken into account the same value as the one used for the ties in section 2 : x_r # 0.05m.

Table 4: Cracking observed in the gusset

Time	Spacing measure	Spacing calcul.	Opening measure	Opening calcul.
t_0+5 days	# 1.2m	-	< 0.1mm	-
t_0+12 days	# 1.2m	1.06m	0.1mm	0.096 mm
t_0+8 months	# 1.2m	-	0.2mm	-

Figure 12 gives the spacing measured on extrados between two ribs (used to locate the prestressing anchors). Table 4 gives the comparison with the one calculated.

Calculated at 12 days, at a stage where maturity is close to one, the average crack spacing value estimated is quite good. Figure 11b shows that damage increase mainly between 2.5 and 5 days which is consistent with the in-situ observations: most of the cracking is formed at 5 days (green line figure 12).

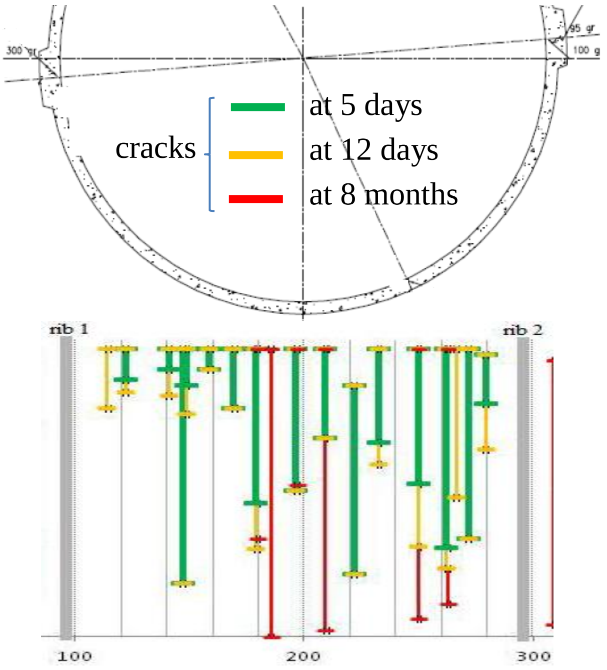

Figure 12: Cracks observed in the gusset presentated in developed form between 100 and 300 grades.

It is also possible to estimate the cracking opening (w_c), from the use of the localized scheme (figure 2) and related to the stress transition zone. From a given crack: at x=0, σ_c=0 and $\varepsilon_c=\varepsilon_r$, at $x=x_r$, $\sigma_c=f_t$ and $\varepsilon_c=\varepsilon_{0t}$, then it comes:

$$w_c = 2\int_0^{x_r}(\varepsilon(x)-\varepsilon_{0t})dx \qquad (32)$$

The linear behavioral curve figure 9a leads to: $w_c=(\varepsilon_r-\varepsilon_{0t}).x_r$, then with ε_r#2.10^{-3} (deduced from (31) for σ_{cm}=0) and x_r#0.05m, w_c=0.096mm, which is a value close to the measured one (cf. table 4).

6 CONCLUSIONS

The aim of the present study was to revisit the way to approach cracking prediction in situations where the stress field is almost homogeneous (tension in a beam or in an axisymmetric reinforced concrete shell).

A simplified approach was proposed, based on an approach where the calculation imposes a diffuse damage. In the same time a localized cracking scheme issued from limit analysis concepts is considered. The dialogue between the two schemes, diffuse and localized, leads to mean cracks indicators (spacing, opening,..).

In a first stage the method was applied to reinforced concrete ties submitted to tensile forces. The results were convincing. Then, in a second stage, the idea was to forecast, with the same procedure, cracking due to early age effects in the gusset of the VeRCoRs mock-up.

To simulate early age effects a complete and efficient modelling previously used in the RG8 test (large RC beam under restrained shrinkage conditions [9]) was applied. The problem is consideed axisymmetric and the various fields (strain, damage,..) in the gusset are assumed quasi homogeneous. The dialogue between the diffuse scheme and the localized one leads to very good cracking indicator values.

The difficulties to forecast the location and the opening of cracks in such a RC structures is well known, even using a 3D approach this needs refined modelling and some probabilistic ingredients. The present modeling is simplified, it leads to results as pertinent as the one obtained in the benchmark VeRCoRs 2015 [2] and moreover the calculation is stable and performed at low cost on the software platform *ATL4S* [16], developed under Matlab and for internal numerical developments. It is initially inspired by the philosophy of FEDEASLAB for data entry [17].

Acknowledgement: the authors would like to thank the EDF VeRCoRs program for providing the experimental results.

REFERENCES

[1] https://fr.xing-events.com/EDF-vercors-project.html, VeRCoRs presentation 2018.

[2] Corbin M., Garcia M., 2015, 1st International Benchmark VeRCoRs - Overview, synthesis and lessons learnt, *EDF report*, Lyon (France).

[3] Boudjiti, D.E., 2018. Analyse probabiliste de la fissuration et du confinement des grands ouvrages en béton armé et précontraints, *PhD report*, Grenoble Alpes University.

[4] Barre F., Bisch P. Chauvel, D. Cortade, J. Dubois, J.P. Erlicher, S. Sellier, A., 2016. Control of Cracking in Reinforced Concrete Structures: *Research Project CEOS.fr;* Ed. by Mazars, J.; ISTE: Wiley, London.

[5] Mayer U. Eligehausen R., 1998. Bond behaviour of ribbed bars at inelastic steel strains, *Proc. 2nd Int. PhD Symposium in Civil Engineering*, Ed. By G. L. Balàzs, Tech. Univ. of Budapest (Hungary) 39-46.

[6] MC2010, fib Model Code for concrete structures 2010 – Ernst & Sohn, Berlin 2013.

[7] Mang C., 2015. Modélisation de la liaison acier-béton dans le calcul des structures en béton armé, *PhD report*, University Paris ouest.

[8] Mivelaz P. 1996. Etanchéité des structures en béton armé : fuite au travers d'un élément fissuré, *PhD report*, EPF Lausanne - Swiss.

[9] Mazars J., Grange S., Briffaut M., 2018 Simplified Modeling Strategy for the Thermomechanical Analysis of Massive Reinforced Concrete Structures at an Early Age, *Applied Sciences*, 8, 448.

[10] Briffaut, M.; Benboudjema, F.; Torrenti, J.M.; Nahas G., 2011. Numerical analysis of the thermal active restrained shrinkage ring test to study the early age behaviour

of massive concrete structures. *Eng. Structures*, *33*, 1390–1401.

[11] Sciumè, G.; Benboudjema, F.; De Sa, C.; Pesavento, F.; Berthaud, Y.; Schrefler, B., 2012. A multi-physics model for concrete at early age applied to repairs problems. *Eng. Structures*, *57*, 374–387.

[12] Mazars, J.; Bournazel, J.P., 1998. Modelling of damage processes due to volumic variations for maturing and matured concrete. In *Concrete from Material to Structure*; Malier, Y., Bournazel, J.-P., Eds.; RILEM 1998; pp. 43–54.

[13] Mazars, J., Hamon, F. and Grange, S., 2015. A new 3D damage model for concrete under monotonic,cyclic and dynamic loading, *Materials and Structures*, 48, 3779-3793.

[14] Lee J., Fenves G.L., 1998. Plastic-Damage Model for Cyclic Loading of Concrete Structures**,** *Journal of Engineering Mechanics* 124, 892**,** 1998.

[15] De Schutter G., 1999. Degree of hydration based Kelvin model for the basic creep of early age concrete. *Materials and Structures* 1999, *32*, 260–265.

[16] Grange, S. *ATL4S*, *2016*. A Tool and Language for Simplified Structural Solution Strategy; *Internal Report*; GEOMAS INSA-Lyon, 2016.

[17] Filippou, F. C. and M. Constantinides (2004). FEDEASLab getting started guide and simulation examples. *NEES grid Report* 22: 2004-2005.